73rd International Astronautical Congress (IAC), Paris, France, 18–22 September 2022.

IAC-22-C1.IPB.34.x72589

Framework for Analyzing the Complex Interactions Between Spacecraft Motion and Slosh Dynamics in Low-G Environments

William J. Elke III[a]*, Jing Pei[b], Carlos M. Roithmayr[c], Ryan J. Caverly[d]

[a] *Department of Aerospace Engineering and Mechanics, University of Minnesota, 110 Union St SE, Minneapolis, Minnesota 55455, United States of America*, elke0011@umn.edu
[b] *Atmospheric Flight & Entry Systems Branch, NASA Langley Research Center, 1 Nasa Dr, Hampton, Virginia 23681, United States of America*, jing.pei-1@nasa.gov
[c] *Vehicle Analysis Branch, NASA Langley Research Center, 1 Nasa Dr, Hampton, Virginia 23681, United States of America*, carlos.m.roithmayr@nasa.gov
[d] *Department of Aerospace Engineering and Mechanics, University of Minnesota, 110 Union St SE, Minneapolis, Minnesota 55455, United States of America*, rcaverly@umn.edu
* Corresponding Author

Abstract

The fuel-to-dry-mass ratio of spacecraft continues to grow as new human spaceflight missions target destinations farther from Earth. Large amounts of liquid propellant can lead to significant coupling between the rigid-body dynamics of the spacecraft and the motion of the fuel within its storage tank. The present work gives an overview of the dynamic features and a flowchart for a method of simulating the motion of a spacecraft with fuel slosh inside a cylindrical, domed tank in a low-g environment. The method involves modeling the liquid propellant as a particle that transfers momentum to the spacecraft through perfectly inelastic collisions with the tank wall. The foundation of the modeling methodology is the approach taken during the Apollo program used to predict the effect of fuel slosh on the complex motion exhibited by the Service Module following separation from the Command Module. This paper discusses the motivation, methodology, and conclusions from the Apollo-era method, then presents corrections to the derivation of the dynamics and fills in the gaps left from the unavailability of the detailed contractor report and simulation code. The results presented in this paper provide an example that demonstrates the effect that fuel slosh can have on the trajectory of a spacecraft in a low-g environment.

Keywords: low-g fuel slosh, spacecraft dynamics, spacecraft guidance, navigation, and control (GN&C), constraints

1. Introduction

Current and future space exploration missions will utilize spacecraft with a large fuel-to-dry-mass ratio. Large amounts of liquid propellant can lead to significant coupling between the rigid-body dynamics of the spacecraft and the motion of the fuel within its storage tank. Of particular interest for this study are the spacecraft-propellant interactions that take place in a low-g environment. In short, small relative accelerations between the spacecraft and its liquid propellants characterize a low-g environment—the technical definition of low-g environments used in this work is found in Refs. [1, 2]. There are many ways this interaction can negatively affect system level requirements and mission success. For instance, it may preclude the attitude control system from achieving the desired pointing accuracy or cause an excessive amount of propellant to be expended. In the event of spacecraft jettison, residual propellant onboard the discarded vehicle may significantly alter the trajectory, resulting in recontact with the vehicle in service. The latter describes what almost transpired during Apollo missions 8, 10, and 11 in which the Service Module (SM) separated from the Command Module (CM) prior to Earth reentry as discussed in Refs. [3, 4]. Crew members onboard the CM observed the jettisoned SM tumbling through their field of view despite the fact that the jettison maneuver was planned in such a way that the SM should have never done so; a visualization of this anomaly is found in Fig. 1 of Ref. [4]. This potentially catastrophic, unintended retrograde motion is attributed to the gross reorientation of the residual propellant inside the tanks of the SM in Ref. [3] and replicated with numerical simulation in Ref. [4]. A similar concern is investigated in Ref. [5] for the STARDUST mission. In Ref. [5], the authors analyze the controlled despin of the spacecraft after separation for the possibility of recontact with the launch vehicle upper stage.

Analyzing the complex interaction between a spacecraft and propellant in a low-g environment is a complicated undertaking and active area of research. The dy-

namic model developed in Ref. [4] appears to be successful in simulating the general motion of the residual propellant inside the tanks and reproducing the observed retrograde motion. Reference [2] uses a single torsional spring-restrained pendulum mechanical analog model to describe the behavior of the low-g slosh dynamics. Pendulum parameters such as spring stiffness, length, and damping are functions of lateral acceleration and fill level. Computational fluid dynamics (CFD) solvers such as Flow-3D are used determine the parameters in off-line simulations. In the vehicle simulation, equivalent force and moments due to slosh are applied to the vehicle; however, this approach fails to capture the coupling in the dynamics between the slosh model and spacecraft bus. Furthermore, according to Ref. [6], CFD codes yield poor results when the applied accelerations are small, such as when large amplitude motions have decayed to small amplitude sloshing. Similar analytical models exist such as the work found in Ref. [7]; however, the issues with the lack of dynamic coupling and reduced validity at small acceleration levels persist. Due to modeling complexity, the Space Launch System Exploration Upper Stage adopts the approach of turning off any slosh models during periods of quiescent flight.

The tractability and simplicity of the particle model have resulted in recent advances. References [8, 9] provide descriptions of the Sloshsat Motion Simulator (SMS) that uses a free-moving pulsating ball inside a spherical cavity to capture the physics behind the momentum transfer between the liquid and the spacecraft. The design objective of SMS was to support development and evaluation of control laws for the Sloshsat spacecraft. Reference [5] describes a constraint surface model similar to Ref. [4] that solves for the constraint forces and applies them to the particle and spacecraft to capture the interaction between the two. Reference [10] describes a three-dimensional constraint surface mechanical model that portrays the liquid as a particle. Three distinct mathematical models are used to describe the dynamics of the coupled system when the particle moves freely inside the tank, collides with the tank walls, or slides along the tank wall. Good comparisons with Flow-3D are shown for a few different values of forced accelerations. Moreover, the constraint surface model shows an improvement in computational time of two orders of magnitude compared to the Flow-3D model. This allows the analyst to rapidly evaluate the design space and assess controller performance without relying on time-consuming CFD solutions. Rather than using the tank geometry as the constraint surface, both Refs. [5, 10] define the constraint surface as the minimum potential energy ellipsoid of the fuel center of mass in a constant acceleration field for all possible tank orientations.

An accurate low-g slosh and spacecraft dynamics model that can run in real time or faster has many space GN&C applications. For instance, the model can be used to assess degradation of handling qualities in the presence of low-g slosh dynamics during manual rendezvous proximity operations and docking events. Furthermore, such a model can be incorporated into an attitude navigation filter for a more accurate representation of the dynamics. Finally, such models would allow controls engineers to quickly assess jettison maneuvers to avoid recontact as demonstrated in Refs. [4, 5].

The novel contribution of this work is the development of a generalized framework for rapidly analyzing spacecraft-propellant interactions in a low-g environment. The methodology closely follows the particle modeling approach described in Ref. [4] with some additional enhancements—heritage and analytical tractability being the top motivating factors. Despite exhausting all available sources, the authors of this work were unable to find the Apollo contractor reports that contain the comprehensive theoretical development [11] and user manual [12] as well as the simulation that produced the results in Refs. [4, 13]. In lieu of this, the authors of this work correct the mistakes found in Ref. [4] and apply the principles of impulse and momentum as a more rigorous approach to the collision dynamics.

The remainder of the paper is organized into three sections. Section 2 discusses the dynamics modeled in Ref. [4] and points out the mistakes and unmodeled dynamics discovered upon review. Section 3 contains an overview of the simulation framework and results from an example. Conclusions are presented in Section 4.

2. Dynamics

This section contains an overview of the dynamics that are modeled in Ref. [4] and applied in Section 3. The discussion covers the mistakes discovered in Ref. [4].

2.1 System Description

In order to understand the modeling choices made in this work, consider the dynamical system from Ref. [4]. This system consists of the Apollo-era SM with an oxidizer tank and a fuel tank, each containing some amount of propellant. The spacecraft is treated as a rigid body with constant mass and inertia properties; the liquids contained in each tank are treated as particles of mass equivalent to the corresponding liquid. The tanks are cylindrical tanks capped with hemispheres on both ends, henceforth referred to as domed tanks. All collisions between the spacecraft and each of the particles are treated as perfectly inelastic collisions. When a particle is in contact with the tank wall, friction forces of equal magnitude and opposite direction tangent to the tank wall are applied to the

spacecraft bus and the particle. The friction model is an empirical model that is a function of particle velocity and normal force.

The work presented here examines a modified version of the system previously described with the following alterations. Although the approach described in Ref. [4] can be generalized for any number of domed tanks with each containing a single particle, the authors decided to limit the scope to a single tank-particle combination in this study. Furthermore, friction forces are ignored but could be readily implemented in the form expressed by Eqns. (18)–(21) of Ref. [4]. The friction coefficients can be adjusted to account for spatial features of the tank such as slosh baffles.

2.2 Equations of Motion

Reference [4] derives the translational and rotational equations of motion of the spacecraft via a Newton-Euler approach. Subsequently, the translational acceleration of the particle is derived using kinematics. The derivation of the translational acceleration of the particle contains some errors; specifically, there are missing terms in Eqns. (10)–(14) of Ref. [4].

Before the mistakes can be highlighted, a definition of points and reference frames is necessary. Consider Fig. 1 that presents a schematic of the system. Point B^* denotes the SM center of mass, point O denotes a point fixed to the center of the intersection between the forward hemispherical and cylindrical portions of the tank, and point P denotes the particle. Note that point B^* does not necessarily lie on the centerline of the spacecraft and that the particle does not have volume despite the size of point P. For the purposes of this paper, the inertial frame $\left(\underrightarrow{X}, \underrightarrow{Y}, \underrightarrow{Z}\right)$, SM body-fixed frame $\left(\underrightarrow{x}, \underrightarrow{y}, \underrightarrow{z}\right)$, and particle tracking frames $\left(\underrightarrow{e}_R, \underrightarrow{e}_M, \underrightarrow{e}_T \text{ and } \underrightarrow{e}_{CR}, \underrightarrow{e}_{CL}, \underrightarrow{e}_{CT}\right)$ used in Ref. [4] are denoted by $\mathcal{F}_i$, $\mathcal{F}_b$, and $\mathcal{F}_e$ respectively. Each of these frames are orthonormal, dextral, and defined by unit vectors. The particle tracking frames $\underrightarrow{e}_R, \underrightarrow{e}_M, \underrightarrow{e}_T$ and $\underrightarrow{e}_{CR}, \underrightarrow{e}_{CL}, \underrightarrow{e}_{CT}$ are spherical and cylindrical coordinate systems used to describe the location of the particle when it is in the hemispherical and barrel sections of the tank respectively. Figure 4 of Ref. [4] presents a visualization of these reference frames.

Equation (5) of Ref. [4] is the expression of the particle's acceleration with respect to $\mathcal{F}_i$ resolved in $\mathcal{F}_b$. This equation is rewritten in vector form (i.e., so that it is not resolved in any frame) as follows.

$$\underrightarrow{a}^{P} = \underrightarrow{a}^{O} + \underrightarrow{\omega}^{bi\bullet b} \times \underrightarrow{r}^{P} + \underrightarrow{\omega}^{bi} \times \underrightarrow{\omega}^{bi} \times \underrightarrow{r}^{P} + 2\,\underrightarrow{\omega}^{bi} \times \underrightarrow{r}^{P^{\bullet b}} + \underrightarrow{r}^{P^{\bullet b \bullet b}}, \tag{1}$$

where $\underrightarrow{a}^{P}$ is the acceleration of the particle with respect to $\mathcal{F}_i$; $\underrightarrow{a}^{O}$ is the acceleration of point O with respect to $\mathcal{F}_i$; $\underrightarrow{\omega}^{bi}$ is the angular velocity of $\mathcal{F}_b$ relative to $\mathcal{F}_i$; $\underrightarrow{\omega}^{bi\bullet b}$ is the time derivative of $\underrightarrow{\omega}^{bi}$ taken with respect to $\mathcal{F}_b$; and, $\underrightarrow{r}^{P}$, $\underrightarrow{r}^{P^{\bullet b}}$, and $\underrightarrow{r}^{P^{\bullet b \bullet b}}$ are the position, velocity, and accelerations of the particle relative to point O, respectively, with all time derivatives taken with respect to $\mathcal{F}_b$.

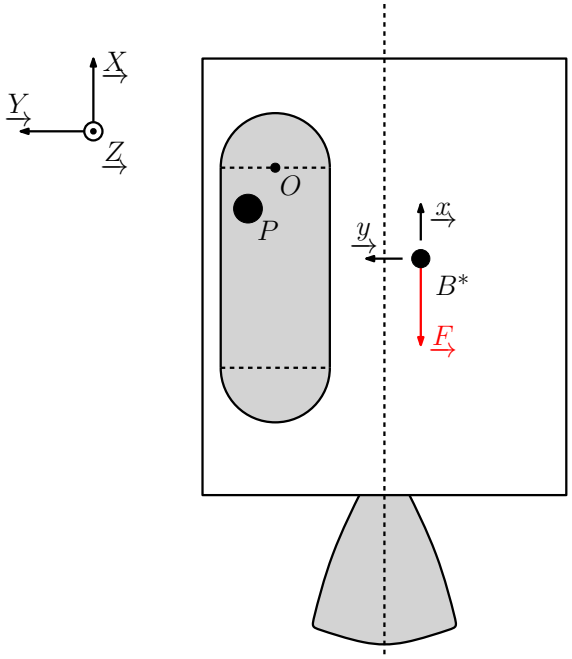

Fig. 1. Schematic of the spacecraft and particle system.

Now consider the application of the transport theorem (p. 23 of Ref. [14] and p. 47 of Ref. [15]) to $\underrightarrow{\omega}^{bi\bullet b}$ in Eqn. (1), resulting in

$$\underrightarrow{\omega}^{bi\bullet b} = \underrightarrow{\omega}^{bi\bullet e} + \underbrace{\underrightarrow{\omega}^{eb} \times \underrightarrow{\omega}^{bi}}_{\text{Missing}}, \tag{2}$$

where $\underrightarrow{\omega}^{bi\bullet e}$ is the time derivative of $\underrightarrow{\omega}^{bi}$ taken with respect to $\mathcal{F}_e$ and $\underrightarrow{\omega}^{eb}$ is the angular velocity of $\mathcal{F}_e$ relative to $\mathcal{F}_b$. This crucial step is left out of Ref. [4] resulting in the omission of the term labeled as "Missing." It appears the authors of Ref. [4] simply set $\underrightarrow{\omega}^{bi\bullet b} = \underrightarrow{\omega}^{bi\bullet e}$ and did not account for the fact that $\mathcal{F}_e$ can rotate relative to $\mathcal{F}_b$.

The consequences of this mistake manifest in Eqns. (10)–(14) of Ref. [4]. Note that Eqn. (9) of Ref. [4] is correct. These scalar equations are a result of taking the dot product between Eqn. (1) and the unit vectors that define $\mathcal{F}_e$. These equations are now presented here with the missing terms, each of which can be traced back to the original omission of the transport term in Eqn. (2). The expressions for the acceleration of the particle resolved in

$\underrightarrow{e}_M$ and $\underrightarrow{e}_T$ (Eqns. (10) and (11) from Ref. [4]) are

$$\begin{aligned}(A_p)_M = {} & (A_0)_M + \dot{\Omega}_T \cdot \rho + \Omega_R \cdot \Omega_M \cdot \rho \\ & + 2\Omega_T \cdot \dot{\rho} - 2\Omega_R \cdot \rho \cdot \dot{\phi} \cdot \sin\theta \\ & + \rho \cdot \ddot{\theta} + 2\dot{\rho} \cdot \dot{\theta} - \rho \cdot \dot{\phi}^2 \cdot \sin\theta \cdot \cos\theta \\ & + \underbrace{\Omega_M \cdot \rho \cdot \dot{\phi} \cdot \cos\theta + \Omega_R \cdot \rho \cdot \dot{\phi} \cdot \sin\theta}_{\text{Missing}}, \end{aligned} \tag{3}$$

$$\begin{aligned}(A_p)_T = {} & (A_0)_T + \dot{\Omega}_M \cdot \rho + \Omega_R \cdot \Omega_T \cdot \rho \\ & + 2\Omega_R \cdot \rho \cdot \dot{\theta} - 2\Omega_M \cdot \dot{\rho} + \rho \cdot \ddot{\phi} \cdot \sin\theta \\ & + 2\dot{\rho} \cdot \dot{\phi} \cdot \sin\theta + 2\rho \cdot \dot{\phi} \cdot \dot{\theta} \cdot \cos\theta \\ & + \underbrace{\Omega_T \cdot \rho \cdot \dot{\phi} \cdot \cos\theta - \Omega_R \cdot \rho \cdot \dot{\theta}}_{\text{Missing}}. \end{aligned} \tag{4}$$

The corrected equations of acceleration of the particle resolved in $\underrightarrow{e}_{CR}$, $\underrightarrow{e}_{CL}$, $\underrightarrow{e}_{CT}$ (Eqns. (12)–(14) from Ref. [4]) are

$$\begin{aligned}(A_p)_{CR} = {} & (A_0)_{CR} - \dot{\Omega}_{CT} \cdot \eta_c - \left(\Omega_{CL}^2 + \Omega_{CT}^2\right) \cdot \rho_c \\ & + \Omega_{CR} \cdot \Omega_{CL} \cdot \eta_c + 2\Omega_{CL} \cdot \rho_c \cdot \dot{\phi} \\ & - 2\Omega_{CT} \cdot \dot{\eta}_c + \ddot{\rho}_c - \rho_c \cdot \dot{\phi}^2 + \underbrace{\Omega_{CR} \cdot \eta_c \cdot \dot{\phi}}_{\text{Missing}}, \end{aligned} \tag{5}$$

$$\begin{aligned}(A_p)_{CL} = {} & (A_0)_{CL} + \dot{\Omega}_{CT} \cdot \rho_c + \Omega_{CR} \cdot \Omega_{CL} \cdot \rho_c \\ & - \left(\Omega_{CR}^2 + \Omega_{CT}^2\right) \cdot \eta_c + 2\Omega_{CT} \cdot \dot{\rho}_c \\ & - 2\Omega_{CR} \cdot \rho_c \cdot \dot{\phi} + \ddot{\eta}_c + \underbrace{\Omega_{CR} \cdot \rho_c \cdot \dot{\phi}}_{\text{Missing}}, \end{aligned} \tag{6}$$

$$\begin{aligned}(A_p)_{CT} = {} & (A_0)_{CT} - \dot{\Omega}_{CL} \cdot \rho_c + \dot{\Omega}_{CR} \cdot \eta_c \\ & + \Omega_{CR} \cdot \Omega_{CT} \cdot \rho_c + \Omega_{CL} \cdot \Omega_{CT} \cdot \eta_c \\ & - 2\Omega_{CL} \cdot \dot{\rho}_c + 2\Omega_{CR} \cdot \dot{\eta}_c \\ & + \rho_c \cdot \ddot{\phi} + 2\dot{\rho}_c \cdot \dot{\phi} + \underbrace{\Omega_{CT} \cdot \eta_c \cdot \dot{\phi}}_{\text{Missing}}. \end{aligned} \tag{7}$$

2.3 Constraints

The discussion up to this point pertains to the case when the particle is free floating and not in contact with the tank wall. Since there are no constraints being enforced, the system has nine degrees of freedom (DOF): three for spacecraft translation, three for spacecraft rotation, and three for particle translation. When the particle is moving along the tank wall, the kinematic constraint in Eqn. (15) of Ref. [4] is applied and the degrees of freedom of the system are reduced by one from 9 DOF to 8 DOF. The constraint prevents particle translation normal to the tank wall. The constraint force acting orthogonal to the tank wall is described by Eqns. (16) and (17) of Ref. [4] when the particle is located inside the hemispherical and cylindrical sections of the domed tank respectively. Reference [4] appears to have excluded a term involving gravitational force in Eqns. (16) and (17) following the stated assumption that the orbital centrifugal force perfectly cancels out the gravitational force.

In this work and Ref. [4], the motion of the particle is restricted to stay on the constraint surface defined by the domed tank's geometry. References [5, 10] describe alternative approaches to model the constraint surfaces based on how the fluid behaves in a one-g environment.

2.4 Collision Dynamics

A collision occurs when the particle makes initial contact with the tank wall. The collision implementation described in Ref. [4] involves first solving the constrained kinematic equation for the acceleration of the particle at the moment of the collision. Using the result from the first step, normal and friction forces having equal magnitudes and opposite directions are computed and applied to the SM and particle. These forces resolved in cylindrical coordinates (Eqns. (17), (20), and (21) of Ref. [4]) are incorrect considering the equation for the radial acceleration of the particle (Eqn. (12) of Ref. [4]) is missing the terms identified in Eqn. (5). Also, there is no evidence that the principles of impulse and momentum were considered for the full scope of the DOF involved. Therefore, it is unclear whether the behavior of the system would be accurate even with correct equations.

The authors of Ref. [4] comment on the numerical sensitivity of the equations of motion, and the authors of the present work believe that their implementation of the collision dynamics is a contributing factor. Their method of implementation is useful for applications such as adding the particle model to an existing rigid body spacecraft simulation. However, a more numerically stable approach exists that incorporates the principles of impulse and momentum discussed in Refs. [14, 15] to solve for the states of the system following a collision. This approach results in discrete changes in system states and requires a variable-size time step solver that may not be applicable in all situations.

The collision problem can be stated as follows: "given the states of the system at the instant prior to the collision and the type of collision, solve for the velocities of the system at the instant following the collision". Nine algebraic equations are derived to solve this problem using the principles of impulse and momentum and the coefficient of restitution derived in Refs. [14, 15]. Consider the equa-

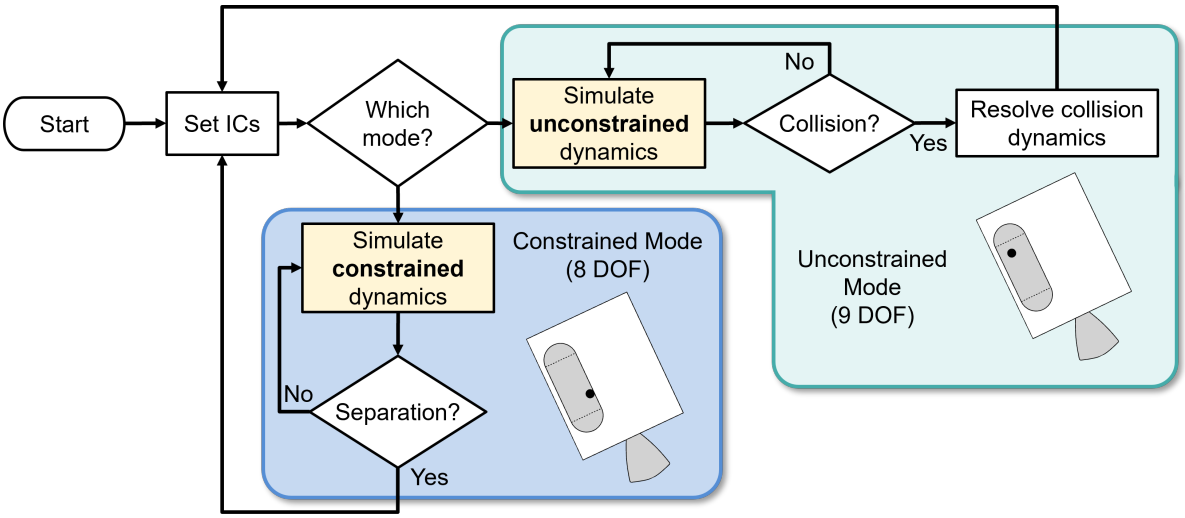

Fig. 2. Block diagram of simulation architecture.

tion for the coefficient of restitution (p. 452 of Ref. [15])

$$\varepsilon = \frac{\left(\underset{\rightarrow}{r}^{p\bullet i}\right)' \cdot \underset{\rightarrow}{n} - \left(\underset{\rightarrow}{r}^{q\bullet i}\right)' \cdot \underset{\rightarrow}{n}}{\underset{\rightarrow}{r}^{q\bullet i} \cdot \underset{\rightarrow}{n} - \underset{\rightarrow}{r}^{p\bullet i} \cdot \underset{\rightarrow}{n}}, \tag{8}$$

where $\underset{\rightarrow}{r}^{p\bullet i}$ is the velocity with respect to $\mathcal{F}_i$ of the particle at the instant prior to the collision, $\underset{\rightarrow}{r}^{q\bullet i}$ is the velocity with respect to $\mathcal{F}_i$ of the point on the tank wall at the location of the collision at the instant prior to the collision, $(\bullet)'$ is velocity vector, $\bullet$, at the instant following the collision, and unit vector $\underset{\rightarrow}{n}$ is $\underset{\rightarrow}{e}_R$ or $\underset{\rightarrow}{e}_{CR}$ depending on the particle's location inside the domed tank. This study and Ref. [4] assume all collisions are perfectly inelastic. This corresponds to setting $\varepsilon = 0$ and results in the relative radial velocity equaling zero after the collision.

Equation (8) provides one algebraic relationship for solving the collision problem. The principles of impulse and momentum, as discussed in Sections 7.8 and 7.9 of Ref. [14] and Section 5.12 of Ref. [15], are applied to obtain the remaining equations.

2.5 Singularities

The reader should be aware that a thorough understanding of the selection and application of a coordinate system is crucial. When choosing cylindrical and spherical coordinates to describe the location of the particle relative to point O, as in Ref. [4], singularities are reached when $\rho = 0$, $\rho_c = 0$, or $\theta = 0$; these singularities are analogous to gimbal lock. In short, when the particle lies on the center axis of the tank, a unique solution for the cylindrical or spherical coordinates does not exist. Reference [4] contains a brief description of the effects of the singularities on the numerical stability of the simulation and notes that the size of the time step was decreased to mitigate the effects. This is a limitation that comes with the use of cylindrical and spherical coordinates and highlights the trade-off that comes with using these intuitive coordinate systems.

3. Simulation & Results

Reference [4] does not provide a wholly satisfactory description of the simulation architecture, particularly for readers unfamiliar with the concepts of enforcement of constraints. What follows is a description of the complete simulation architecture supplemented by a flowchart and results from an example. Reference [16] establishes the framework for the enforcement and relaxation of constraints implemented in this work.

3.1 Simulation Architecture

The simulation framework—based upon the considerations discussed in Section 2—has two operating modes. The Unconstrained Mode is active when the particle moves freely and is not in contact with the tank wall, whereas the Constrained Mode is utilized when the particle slides along the tank wall. Figure 2 provides a flowchart of the simulation architecture.

The simulation begins with initial conditions specified by the user. This includes the spacecraft position, attitude, velocity, and angular velocity, as well as the particle position and velocity. A flag indicating the mode in which the simulation starts is also initialized. Once the initialization is completed, the simulation checks the flag to see if the Unconstrained Mode or Constrained Mode should be used.

The Unconstrained Mode begins by numerically in-

tegrating the 9 DOF unconstrained equations of motion described in Section 2. Simultaneously, it is also continuously checking for a collision between the tank wall and particle. If there is no collision detected, the simulation continues numerical integration of the unconstrained equations of motion. Once a collision is detected, the value of the states immediately following the collision are computed algebraically using the principles of impulse and momentum described in Section 2, the flag is set to indicate that the Constrained Mode must be activated, and the simulation exits the Unconstrained Mode. The simulation then returns to the beginning of the flowchart where the initial conditions are reset to the values following the collision.

The Constrained Mode begins by numerically integrating the 8 DOF constrained equations of motion described in Section 2. Simultaneously, the normal force between the wall and particle is computed at each time step. If the normal force is tensile, then a separation occurs. Otherwise, the simulation continues numerical integration of the states using the constrained equations of motion. Once a separation is detected the flag is set to indicate that the Unconstrained Mode must be activated. The simulation then exits the Constrained Mode and returns to the beginning of the flowchart where the initial conditions are reset to the states at the time step immediately preceding the separation.

The exchange between the Unconstrained and Constrained Modes continues until the user-specified terminal simulation time is reached.

3.2 Numerical Example

An example is presented that demonstrates simulation capabilities. This notional example involves a stationary spacecraft with an initial angular velocity and a prescribed open-loop thrust profile lasting 30 seconds. Fig. 1 presents a schematic of the system at $t = 0$ s for a single case. The simulation is run multiple times, with varying conditions of the particle. This is done to highlight the effects fuel slosh can have on the motion of the spacecraft in a low-g environment.

The spacecraft in the simulation has the same mass properties as the SM in Ref. [4], but has only one domed tank instead of two. The spacecraft is stationary at $t = 0$ s and has an initial angular velocity in the x direction of 18 deg/s. The spacecraft follows a thrust profile that begins with the reaction control system thrusters firing in the negative x direction at $t = 0$ s; the thrusters shut off at $t = 15$ s. The thruster dynamics are not modeled and the resultant force $\underrightarrow{F}$ is applied at point B^*. The center of mass of the spacecraft is not located on the x axis, as seen in Fig. 1, which is consistent with the configuration provided in Ref. [4].

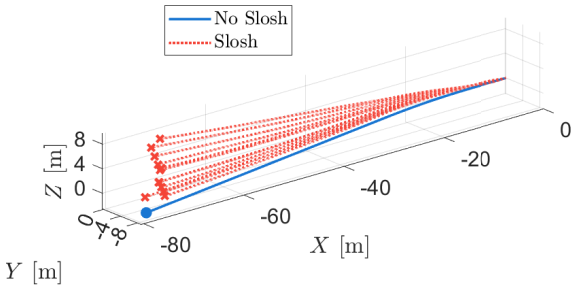

(a) Three-dimensional time histories of B^*.

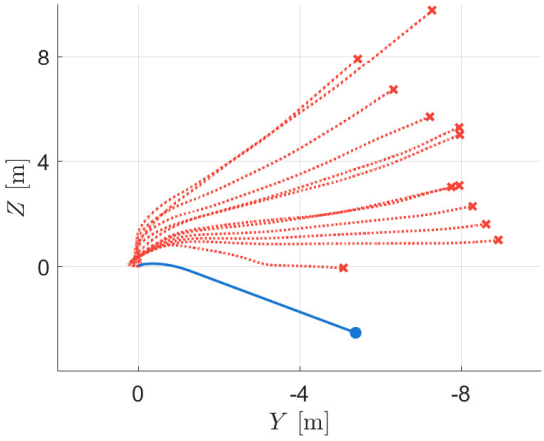

(b) Projection of Fig. 3a onto the YZ plane. Positive $\underrightarrow{X}$ points into the page.

Fig. 3. Spacecraft trajectory results from numerical example over 30 seconds.

The resulting trajectories can be seen in Fig. 3. Figure 3a shows a three-dimensional view of the time history of the position of point B^*. The solid blue line represents the no-slosh case, whereas the dashed red lines represent cases with various initial positions and velocities of the particle. The initial velocities of the particle have magnitudes in the range 0 to 11 in/s. Figure 3b shows the projection of the trajectories onto the YZ plane.

The ensemble of trajectories after 30 seconds shown in Fig. 3b demonstrates the importance of capturing the interactions between fuel slosh and spacecraft. For the assumed parameters and open-loop thrust profile, deviations in the final position of point B^* can be as much as 10 m in magnitude. A review of the system's energy and momenta verified the validity of the equations of mo-

tion. The system's energy increases when the thrusters are on and conserved when the thrusters are off, provided no collisions occur. The system experiences discrete energy losses whenever a collision occurs. The system's translational and angular momenta are conserved when the thrusters are off, but not conserved when the thrusters are on.

4. Conclusions

A framework for predicting the complex interactions between fuel slosh and spacecraft in a low-g environment is described in this paper along with historical context. The study is motivated by the methodology developed during Project Apollo as engineers sought to predict the unintended retrograde motion displayed by the SM following separation from the CM, prior to Earth reentry. Detailed contractor reports of the simulation are lost; thus, the authors of this work recreate the system dynamics from first principles based on the limited information provided in Ref. [4]. Along the way, several mistakes are identified in Ref. [4] and presented here. The contemporary simulation flowchart is discussed and results from an example application are presented. Results highlight the effects liquid propellant can have on the gross motion of a spacecraft in a low-g environment. The simulation framework presented in this study serves as a platform for analyzing the underlying dynamics behind the complex interaction between a spacecraft and its liquid propellant.

Acknowledgments

This material is based upon work supported by the NASA Office of STEM Engagement (OSTEM) under Grant No.80NSSC19K1672 issued through the NASA Fellowships Program under MUREP funding.

References

[1] F. T. Dodge, *The New "Dynamic Behavior of Liquids in Moving Containers"*, Southwest Research Institute, 2000.

[2] P. J. Enright and E. C. Wong, "Propellant Slosh Models for the Cassini Spacecraft," *Astrodynamics Conference*, pp. 186–195, 1994.

[3] "MSC-03466, Apollo 11 Mission Anomaly Report No. 3, Service Module Entry, November 1970," *NASA Apollo 11 Technical Crew Debriefing*, vol. II, Jul. 1969.

[4] D. H. Merchant, R. M. Gates, and J. F. Murray, "Prediction of Apollo Service Module Motion after Jettison," *Journal of Spacecraft and Rockets*, vol. 8, pp. 587–592, 1971.

[5] P. G. Good, A. Carpenter, H. Flanders, and T. Gardner, "STARDUST TCM and Despin in the Presence of Complex Fuel Dynamics," *Advances in the Astronautical Sciences*, vol. 99, pp. 611–628, Feb. 1998.

[6] F. T. Dodge, S. T. Green, and D. D. Kaña, "Fluid Management Technology: Liquid Slosh Dynamics and Control," *NASA-CR-189107*, Nov. 1991.

[7] J. W. Jang, A. Alaniz, L. Yang, J. Powers, and C. Hall, "Mechanical Slosh Models for Rocket-Propelled Spacecraft," *AIAA Guidance, Navigation, and Control (GNC) Conference*, Aug. 2013.

[8] J. P. B. Vreeburg, "Dynamics and Control of a Spacecraft with a Moving Pulsating Ball in a Spherical Cavity," *Acta Astronautica*, vol. 40, pp. 257–274, 1997.

[9] J. P. Vreeburg and D. J. Chato, "Models for Liquid Impact Onboard Sloshsat FLEVO," *AIAA Space Conference and Exposition*, Sep. 2000.

[10] Z. Zhou and H. Huang, "Constraint Surface Model for Large Amplitude Sloshing of the Spacecraft with Multiple Tanks," *Acta Astronautica*, vol. 111, pp. 222–229, 2015.

[11] R. Gates and D. Merchant, "General Motion of a Rigid Spacecraft with Fluid Reorientation—Theoretical Manual," *D2-118301-1*, The Boeing Co., Houston, Texas, May 1970.

[12] J. Murray, "General Motion of a Rigid Spacecraft with Fluid Reorientation—Computer User's Manual," *D2-118301-2*, The Boeing Co., Houston, Texas, May 1970.

[13] D. Merchant and R. Gates, "CM-SM Separation Dynamics," *5-2961-HOU-107*, The Boeing Co., Houston, Texas, Dec. 1969.

[14] T. R. Kane and D. A. Levinson, *Dynamics: Theory and Applications*, McGraw-Hill, 1985.

[15] A. V. Rao, *Dynamics of Particles and Rigid Bodies*, Cambridge University Press, 2006.

[16] S. Djerassi, "Imposition of Constraints," *Journal of Applied Mechanics*, vol. 61, pp. 434–439, Jun. 1994.